BIOCHEMISTRY
including biophysical chemistry & molecular biology

Article

pubs.acs.org/biochemistry

Allosteric Breakage of the Hydrogen Bond within the Dual-Histidine Motif in the Active Site of Human Pin1 PPIase

Jing Wang,[†] Naoya Tochio,[‡] Ryosuke Kawasaki,[†] Yu Tamari,[†] Ning Xu,[†] Jun-ichi Uewaki,[‡] Naoko Utsunomiya-Tate,[§] and Shin-ichi Tate*[,†,‡]

[†]Department of Mathematical and Life Sciences, School of Science, Hiroshima University, 1-3-1 Kagamiyama, Higashi-Hiroshima 739-8526, Japan

[‡]Research Center for the Mathematics on Chromatin Live Dynamics (RcMcD), Hiroshima University, 1-3-1 Kagamiyama, Higashi-Hiroshima 739-8526, Japan

[§]Faculty of Pharma-Sciences, Teikyo University, 2-11-1 Kaga, Itabashi-ku, Tokyo 173-8605, Japan

Supporting Information

ABSTRACT: Intimate cooperativity among active site residues in enzymes is a key factor for regulating elaborate reactions that would otherwise not occur readily. Peptidyl-prolyl *cis-trans* isomerase NIMA-interacting 1 (Pin1) is the phosphorylation-dependent *cis-trans* peptidyl-prolyl isomerase (PPIase) that specifically targets phosphorylated Ser/Thr-Pro motifs. Residues C113, H59, H157, and T152 form a hydrogen bond network in the active site, as in the noted connection. Theoretical studies have shown that protonation to thiolate C113 leads to rearrangement of this hydrogen bond network, with switching of the tautomeric states of adjacent histidines (H59 and H157) [Barman, A., and Hamelberg, D. (2014) *Biochemistry* 53, 3839−3850]. This is called the "dual-histidine motif". Here, C113A and C113S Pin1 mutants were found to alter the protonation states of H59 according to the respective residue type replaced at C113, and the mutations resulted in disruption of the hydrogen bond within the dual-histidine motif. In the C113A mutant, H59 was observed to be in exchange between ε- and δ-tautomers, which widened the entrance of the active site cavity, as seen by an increase in the distance between residues A113 and S154. The C113S mutant caused H59 to exchange between the ε-tautomer and imidazolium while not changing the active site structure. Moreover, the imidazole ring orientations of H59 and H157 were changed in the C113S mutant. These results demonstrated that a mutation at C113 modulates the hydrogen bond network dynamics. Thus, C113 acts as a pivot to drive the concerted function among the residues in the hydrogen bond network, as theoretically predicted.

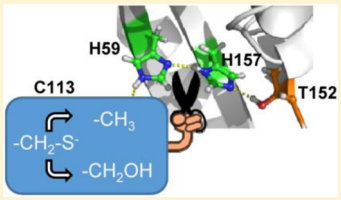

Peptidyl-prolyl *cis-trans* isomerases (PPIases) constitute a family of enzymes that catalyze the inversion of a peptide bond preceding a proline residue in their target proteins.[1,2] Peptidyl-prolyl *cis-trans* isomerase NIMA-interacting 1 (Pin1) is a member of the parvulin family of PPIases that specifically rotates the ω bond of a Pro that is preceded by phosphorylated Ser (pSer) or phosphorylated Thr (pThr). Ser/Thr-Pro motifs are phosphorylated by Pro-directed protein kinases.[3] The Pro-directed protein kinases function in a coupled fashion with Pin1 isomerization of pSer/pThr-Pro motifs to regulate diverse signaling processes in cells.[4−6] Thus, dysfunction of Pin1 is implicated in various diseases, which makes Pin1 a potential therapeutic target.[7−10]

Pin1 consists of two domains, a phosphor-peptide binding domain (WW domain) and a catalytic domain (PPIase domain), and the domains are linked by a flexible unstructured segment.[11] The crystal structure of Pin1 in complex with an Ala-Pro peptide provided insights into how the PPIase domain binds its target motif, although the bound peptide does not contain the canonical pSer/pThr-Pro motif.[11] In the crystal structure, the sulfate ion is captured by basic residues K63, R68, and R69 in the active site loop.[11] The crystal structure revealed that the sulfate ion was located in the corresponding position of the phosphate moiety in the canonical pSer/pThr-Pro motif.[11] Therefore, the three basic residues engage in substrate binding and are termed the "basic triad". The role of the basic triad in phosphate recognition was confirmed by the crystal structure of the Pin1 PPIase domain in complex with a ligand-mimicking inhibitor.[12] In this crystal structure, Pro in the motif is positioned within the hydrophobic pocket comprised of F134, M130, and L122.[11] Ionizable residues C113, H59, and H157 surround the target Pro peptide bond of the substrate.[11]

From the crystal structure of Pin1 PPIase, C113 was proposed to attack the substrate as a nucleophile.[11] In the mechanism, deprotonation of the C113 thiol by the spatially neighboring H59 imidazole ring allows nucleophilic attack of the carbonyl carbon of the substrate peptide to promote *cis−trans* isomerization.[11] However, site-directed mutations of C113 gave controversial results that did not support this mechanism.[11,13] Despite the lack of a nucleophilic group, the C113A mutant maintains catalytic activity, although its catalytic efficiency measured by k_{cat}/K_m is reduced by 130-fold, where k_{cat} is the turnover rate of an enzyme−substrate complex to

Received: June 3, 2015
Revised: July 27, 2015
Published: July 30, 2015

DOI: 10.1021/acs.biochem.5b00606
Biochemistry 2015, 54, 5242−5253

produce the product and K_m is the Michaelis constant.[11] In addition, the C113D and C113S mutants retain isomerization activity without the nucleophile attack moiety, although their catalytic efficiencies were much lower than that of the wild type.[13] The results from these mutant studies challenged the general reaction mechanism of covalent attachment of C113.

Studies using kinetic isotope effects proposed a more feasible mechanism, in which the twisted amide configuration that occurs at a transition state in the isomerization reaction is stabilized by intramolecular hydrogen bonding within the substrate, as found for other types of PPIases, including FKBP and cyclophilin.[14,15] The mechanism does not assume nucleophilic attack by C113 but emphasizes the importance of the proper positioning of the active site residues around the substrate. In particular, the basic triad binding to the phosphor moiety and Q131 hydrogen bonding to the carbonyl oxygen of Pro of the substrate are clearly explained.[14]

The high-resolution crystal structure of Par14, a Pin1 homologue, demonstrated that the ionizable residues in the active site form a hydrogen bond network running across the active site.[16] The residues in the hydrogen bond network are structurally superpositioned to C113, H59, H157, and T152 (listed in the connecting order in the hydrogen bonding network) in Pin1 (in Scheme 1, the residue numbers in Pin1 are in parentheses).[16] Par14 has aspartate instead of cysteine at position 113.[16] A C113D mutant Pin1 PPIase, mimicking the Par14 active site, was shown to have a reduced rate of isomerization relative to that of the wild type.[17] Nuclear magnetic resonance (NMR) analysis showed that D113 formed a tighter hydrogen bond with H59 via the carboxylate oxygen in D113 while the hydrogen bond between H59 and H157 was destabilized.[17] Unbalancing the hydrogen bond network destabilizes the active site structure, which leads to a disorganized basic triad structure in the active loop. The allosteric structural change to the basic triad may explain the reduced level of binding of the C113D mutant to the phosphor-peptide and thereby explain the lowered isomerization rate.[17] These results for the C113D mutant have shown that the correct hydrogen bond network (C113−H59−H157−T152) is essential for efficient isomerization.[17]

Scheme 1

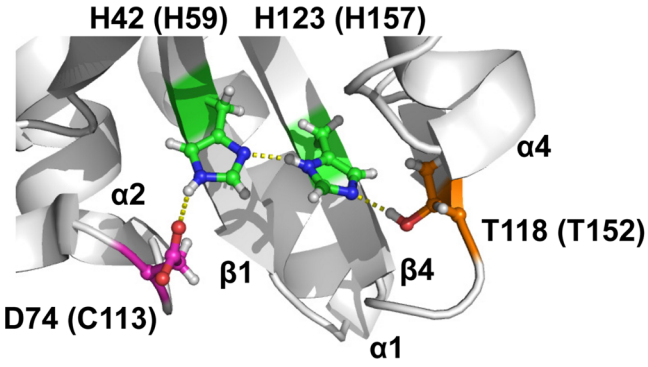

The nucleophile attack of the thiolate in C113 does not seem plausible. Nonetheless, the high chemical reactivity of C113 suggests that C113 stays in a thiolate form in Pin1: Juglone (5-hydroxynaphthoquinone) selectively forms a covalent bond with C113 while keeping C57 intact in Pin1,[18] and C113 is oxidized during storage of purified Pin1 at 4 °C under conditions that leave C57 unmodified.[19] The role of the C113 thiolate in the context of the hydrogen bond network was proposed by Barman and Hamelberg.[20] In their study using free energy calculations and molecular dynamics simulations, they theoretically showed that C113 should stay in a thiolate form in the absence of a substrate, while C113 will be protonated in the substrate-bound complex.[20] The results of the simulations indicated that different protonation states of C113 will change the tautomeric state of the spatially neighboring H59, and this altered tautomerism of H59 will further change the H157 tautomeric state, which subsequently rearranges the hydrogen bonding interaction between H157 and T152.[20] They emphasized that the C113-triggered cooperative protonation change among residues in the hydrogen bond network can energetically explain the *cis*−*trans* isomerization in the active site of Pin1 PPIase.[20]

C113-mediated dynamic rearrangement of the hydrogen bonding network, which Barman and Hamelberg proposed, relies on coupled changes in the protonation states of spatially neighboring H59 and H157; these histidines are conserved among the parvulins and, thus, are termed the "dual-histidine motif".[20] The imidazole ring of histidine has two nitrogen atoms, $N^{\varepsilon 2}$ and $N^{\delta 1}$. The imidazole ring can be in two neutral forms and a charged state according to the pH and/or the local environment. The two neutral imidazole forms are designated as the δ-tautomer (protonated at $N^{\delta 1}$) and the ε-tautomer (protonated at $N^{\varepsilon 2}$), according to the protonated position. In the charged state, the two nitrogen atoms are protonated to form a cationic imidazole ring (imidazolium). In general, protonation of histidine is not observed clearly in X-ray crystal structures. Instead, NMR can discriminate the three states of the imidazole ring on the basis of the $^{15}N^{\varepsilon 2}$ and $^{13}C^{\delta 2}$ chemical shifts that significantly change according to the protonation states.[21,22] Therefore, the C113-mediated dynamic changes in protonation to the dual-histidine motif can be monitored by NMR, which motivated us to study the dynamic rearrangement of the hydrogen bond network by changing the amino acid type at position C113.

C113A and C113S Pin1 PPIase mutants were used in this study. Both mutants have ∼10% enzyme catalytic efficiencies relative to that of the wild-type protein.[13,23] In the context of the C113 mediating the hydrogen bond dynamics by Barman and Hamelberg, the C113S mutant mimics the thiol form of C113 whereas the C113A mutation models the active site structure with a disrupted C113−H59 hydrogen bond. Using the mutants, we intended to see how the change in C113 modulates the active site structure and dynamics through altering protonation to H59 and H157. We found that each mutation of C113 caused different changes to the protonation state of H59. In both mutants, the change in the protonation state of H59 disrupts the hydrogen bond between H59 and H157. The disruption of the hydrogen bond network explains the reduced structural stabilities of both proteins relative to the C113D mutant. The C113D mutant maintains the hydrogen bond network and moderately reduces the structural stability of the active site.[17]

Overall, we observed that the structure and dynamics of the conserved histidines, H59 and H157, were sensitive to changes in the residue type at position 113 of Pin1 PPIase. These results support the theoretical description that the hydrogen bond network, including the dual-histidine motif, is dynamically modulated according to the chemical state of C113. Thus, C113 functions as a trigger to reorganize hydrogen bonds cooperatively within the network of the active site of Pin1.

DOI: 10.1021/acs.biochem.5b00606
Biochemistry 2015, 54, 5242−5253

MATERIALS AND METHODS

Pin1 Sample Preparation. The cDNA encoding the peptidyl-prolyl isomerase (PPIase) domain of human Pin1 (residues 51−163) was cloned into an expression vector, as described previously.[17] Site-directed mutagenesis to change C113 to A or S in the Pin1 PPIase domain was conducted by KOD FX (Toyobo, Osaka, Japan). Expression and purification of the C113A and C113S Pin1 PPIase mutants were conducted as described previously.[17]

Thermal Stability Tests of the Mutant PPIases by Circular Dichroism (CD). The change in the molar ellipticity at 222 nm was used to monitor the thermal denaturing process on a JASCO-720W spectrometer. The sample buffer consisted of 50 mM sodium phosphate (pH 6.0), 100 mM Na_2SO_4, and 1 mM dithiothreitol (DTT). The protein concentration was adjusted to 2 μM. The temperature range was 20−80 °C with an increment rate of 1 °C/min.

NMR Spectroscopy and Structure Determination. Structures of the C113A and C113S Pin1 PPIase mutants were determined according to standard methods using uniformly ^{13}C- and ^{15}N-labeled samples.[24] All NMR data were collected on a Bruker Avance II spectrometer equipped with a triple-resonance cryogenic probe operating at 700.33 MHz for the ^{1}H resonance frequency. For both mutants, protein material was dissolved in a buffer consisting of 50 mM sodium phosphate (pH 6.6), 100 mM Na_2SO_4, 5 mM ethylenediaminetetraacetic acid (EDTA), 1 mM DTT, and 0.03% NaN_3. The protein concentrations were adjusted to 1.0 mM for C113A and 0.4 mM for C113S; the solubility of the C113S mutant was limited. The sample temperature was 299 K for the NMR experiments unless otherwise noted. Data processing and analysis were performed with NMRPipe[25] and KUJIRA[26] running with NMRview,[27] respectively. The CYANA utility was used to perform automated NOE assignments.[28,29] Backbone dihedral angle restraints were generated with TALOS +.[30] The 50 lowest-target function CYANA structures were subjected to explicit water refinement using XPLOR-NIH with distance and dihedral restraints.[31] The 10 lowest-energy structures from the XPLOR-NIH calculation were validated with PROCHECK-NMR.[32] The structural statistics of the C113A and C113S mutants are summarized in Table S1. PyMOL (DeLano Scientific, San Carlos, CA) and MOLMOL[33] were used for the structural analyses and generation of figures.

The resonance assignments and the structural data for the C113A and C113S mutants were deposited in the Biological Magnetic Resonance Bank (BMRB) and Protein Data Bank (PDB), respectively. BMRB accession codes are 11587 for C113A and 11588 for C113S. PDB entries are 2RUQ for C113A and 2RUR for C113S. The backbone ^{1}H−^{15}N resonance assignments of the heteronuclear single-quantum correlation (HSQC) spectra for the mutants are listed in Figure S1.

***cis*−*trans* Isomerization Rates.** The *cis*−*trans* isomerization rates for C113A and C113S mutants were determined by two-dimensional (2D) ^{1}H−^{1}H exchange spectroscopy (EXSY).[34,35] The sample contained 2 mM Cdc25C phosphopeptide with 50 μM PPIase mutant (C113A or C113S). The sample solution contained 50 mM Tris-HCl (pH 6.8), 1 mM DTT, and 0.03% NaN_3. The experiments were performed at 295 K. The mixing times (t_{mix}) were set to 2, 5, 10, 15, 25, 35, 50 (twice), 75, 100 (twice), 200, 300, and 400 ms. The net exchange rate, k_{EX}, was estimated to fit eq 1 to the ratios of the *trans*−*cis* exchange cross-peaks against the *trans* diagonal peaks. In estimating the k_{EX} values, we simultaneously used the buildup profiles from the signals for pT5 CH_3, pT5 HN, and V7 HN for fitting, as in a global fitting manner.

$$\text{ratio}(t_{mix}) = \frac{[1 - e^{-(k_{CT}+k_{TC})t_{mix}}]k_{TC}}{k_{CT} + k_{TC}e^{-(k_{CT}+k_{TC})t_{mix}}} \quad (1)$$

where k_{CT} and k_{TC} are adjustable parameters in the fitting routine and the net exchange rate, k_{EX}, is defined as $k_{EX} = k_{CT} + k_{TC}$, where k_{CT} and k_{TC} are the exchange rates from *cis* to *trans* and from *trans* to *cis*, respectively.[34] Uncertainties in the rate constants were estimated by Monte Carlo simulations on the basis of the duplicate mixing time points.

NMR Spin Relaxation Experiments. All backbone ^{15}N R_1 and R_2 relaxation rates and steady state {^{1}H}−^{15}N heteronuclear NOE (hNOE) data were collected on a 700 MHz NMR spectrometer at 299 K.[36] For the determination of the R_2 relaxation rates, we adopted a composite-type CPMG loop to alleviate off-resonance artifacts.[37] Each peak intensity was measured by averaging over the signal intensities at the peak center and its eight surrounding points (nine-point averaging); each peak center was found by the SPARKY "pc" function (T. D. Goddard and D. G. Kneller, *SPARKY* 3, University of California, San Francisco). The delays for R_1 measurements (t_{relax}) were 10.3 (twice), 153.9, 307.9, 461.8, 615.7 (twice), 769.6, 923.6, 1128.8, and 1539.3 ms, whereas the delays for R_2 (t_{relax}) were 0.0, 16.0 (twice), 40.0, 80.0 (twice), and 160.0 ms. The spectra for R_1 and R_2 were collected in an interleaved manner. For measuring hNOEs, we recorded an interleaved pair of spectra in which ^{1}H saturation for 3 s was applied alternatively with the relaxation delay set to 2 s. R_1 and R_2 relaxation rate constants for each signal were determined using the modelXY TCL built-in function of NMRPipe.[25] Uncertainties for R_1 and R_2 were estimated in a Monte Carlo manner on the basis of the duplicated data points. The uncertainty for each hNOE value was evaluated using the root-mean-square deviation (rmsd) value of a spectral region with no peaks, which was obtained by the NMRPipe built-in module.[35] The reduced spectral density functions, including $J_{eff}(0)$, $J(\omega_N)$, and $J(\omega_h)$, were calculated using the software suite RELAX.[38,39]

H/D Exchange Rates. The amide proton/deuteron exchange (H/D exchange) rates were measured with extensively lyophilized samples; the sample solution [the C113A or C113S Pin1 PPIase mutant in 50 mM sodium phosphate (pH 6.6), 100 mM Na_2SO_4, 5 mM EDTA, 1 mM DTT, and 0.03% NaN_3] was rapidly frozen in liquid nitrogen and placed in a vacuum chamber for approximately 12 h. The lyophilized sample was dissolved with the same volume of D_2O as it was before lyophilization and just prior to recording a series of 2D ^{1}H−^{15}N HSQC spectra. The NMR spectra were initiated within 10 min of the sample being dissolved. One spectrum was collected for 35 min, and 35 data sets were collected sequentially. No apparent spectral difference was observed between the data before and after lyophilization, which ensures the sample preparation had no structural impact on the mutants. H/D exchange rates were determined using the peak intensities of the series of 2D spectra, as described previously.[17]

DOI: 10.1021/acs.biochem.5b00606
Biochemistry 2015, 54, 5242−5253

RESULTS

The C113S Mutant Has an Isomerization Rate Slower Than That of the C113A Mutant. EXSY experiments were used to determine the isomerization rates for the C113A and C113S mutants[17,34] (Figure 1). The C113A mutant showed

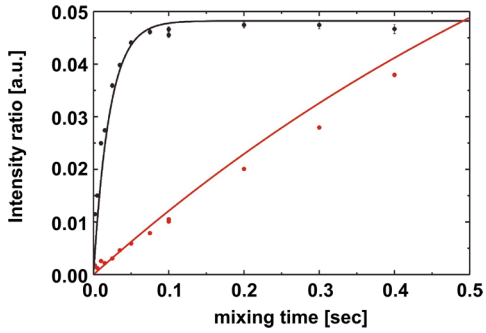

Figure 1. Determination of the isomerization rate with a series of EXSY spectra. The growth of the intensity ratios of the *trans*−*cis* exchange cross-peaks against the diagonal peaks for the *trans* species is plotted for the C113A mutant (red circles). The theoretical fit to the experimental data is presented as a red line. For reference, the corresponding data previously reported for the wild type are included (black circles and black line).[17]

reduced but measurable rates of isomerization as determined by EXSY (Table 1). The isomerization rates were not determined

Table 1. Reduced Global Structural Stabilities and *cis*−*trans* Isomerization Rates of C113A and C113S Pin1 PPIase Mutants

Pin1 PPIase	denaturation temperature (°C)[a]	exchange rate from *cis* to *trans* (k_{CT}) (s^{-1})[b]	exchange rate from *trans* to *cis* (k_{TC}) (s^{-1})[b]
C113A	43.2	1.0 ± 0.2	0.1 ± 0.1
C113S	43.6	not detected	not detected
wild-type[c]	49.4	51.6 ± 1.9	6.6 ± 2.1
C113D[c]	46.2	0.7 ± 0.5	0.1 ± 0.0

[a]Denaturation temperature estimated by the CD molar ellipticity signal at 222 nm. [b]Isomerization exchange rates were directly determined using EXSY experiments. [c]These values were determined in our previous study.[17]

for the C113S mutant; no exchange signals were observed in the spectra with a mixing time of up to 1 s (Figure 1). Thus, the C113S mutant has a *cis*−*trans* isomerization rate, k_{CT}, of <1 s^{-1} (Table 1).

Previous protease-free assays for determining the C113A and C113S catalytic efficiencies (k_{cat}/K_m) gave values of 6 and 4% relative to that of the wild-type protein, respectively.[23] This is consistent with the NMR results that showed that the C113S mutant has isomerization activity lower than that of the C113A mutant (Table 1).

The C113A Mutant Has a Greater Structural Impact on the Spatially Distant Residues in the Hydrogen Bond Network. The backbone ^{1}H and ^{15}N chemical shift changes, $\Delta\delta$, caused by C113A and C113S mutations were compared (Figure 2). Both mutants showed similar $\Delta\delta$ profiles, demonstrating the obvious spectral changes for residues in the β1 strand, β3−β4 loop, and β4 strand, which includes residues engaged in the C113−H59−H157−T152 hydrogen bond network (Figure 2, right).[16] This observation shows that

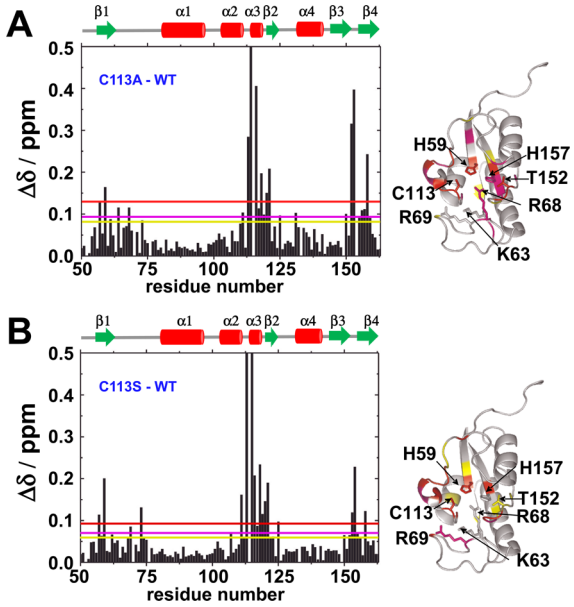

Figure 2. Chemical shift differences for the C113A and C113S mutants relative to the wild-type protein. (A) Normalized chemical shift differences between the wild type and the C113A mutant (left). The normalized chemical shift difference for each residue is defined as $\Delta\delta = [(\Delta\delta^1\mathrm{H})^2 + (\Delta\delta^{15}\mathrm{N}/5)^2]^{1/2}$, where $\Delta\delta^1$H and $\Delta\delta^{15}$N are the chemical shift differences in the ^{1}H and ^{15}N dimensions, respectively.[46] According to the magnitude of $\Delta\delta$, the residues in Pin1 PPIase structure (PDB entry 1PIN)[11] were colored differently: red for greater than $\Delta\delta_{ave} + 1\sigma$, magenta for greater than $\Delta\delta_{ave} + 0.5\sigma$, and yellow for greater than $\Delta\delta_{ave} + 0.25\sigma$, where $\Delta\delta_{ave}$ is the average value for $\Delta\delta$ and σ is the standard deviation of $\Delta\delta$ calculated over all residues (right). The residues in the hydrogen bond network and the basic triad are drawn as stick models with residue names labeled. (B) Plot of $\Delta\delta$ for the C113S mutant (left). Mapping of the chemical shift differences onto the structure using the same criteria presented above (right).

structural perturbation by the C113 mutation, as evidenced by the spectral changes, propagates through the hydrogen bond network. Thus, the C113 mutation disturbs all residues in the network, irrespective of their spatial distance from the mutation site in the α2−α3 loop.

It is noted that the C113A mutant caused spectral changes for residues in the β3−β4 loop and β4 strand greater than the corresponding spectral changes observed for the C113S mutant (Figure 2). The C113A mutation has a greater structural impact than the C113S mutation.

A comparison of the solution structures of the wild-type, C113A, and C113S Pin1 PPIase domains supports the spectral changes. The C113A mutant induces significant structural changes in the β3−β4 loop and β4 when compared with the corresponding parts in the wild-type and C113S structures (Figure S2A).

C113A and C113S Mutations Change the Basic Triad Structure That Binds the Phosphor Moiety. Both the C113A and C113S mutants changed the basic triad structure when compared with that of the wild-type protein (Figure 3). The basic triad interacts with the phosphate moiety upon Pin1 binding the substrate.[14] The structural change to the basic triad in the C113A and C113S mutants explains the reduced binding affinity for the phosphor substrate. Here, binding of the mutants to the substrate was too weak to measure by isothermal titration calorimetry (ITC). This was also observed for the C113D mutant: the basic triad structure was changed,

DOI: 10.1021/acs.biochem.5b00606
Biochemistry 2015, 54, 5242−5253

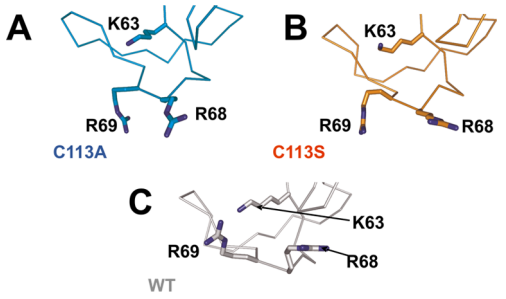

Figure 3. Close-up views of the active loop harboring the basic triad in the Pin1 PPIase domain for the (A) C113A (cyan) and (B) C113S (orange) mutants with (C) the wild type (gray). The residues in the basic triad are drawn as sticks.

and thus, this mutant shows severely reduced substrate affinity such that ITC cannot detect substrate binding.[17]

The active loop ($\beta1-\alpha1$ loop) harboring the basic triad in the C113S mutant has a rigid backbone structure showing hNOE values of >0.8 (Figure S3A). The C113A mutant also has a rigid active loop except for the C-terminal part, i.e., residues W73−Q75, which has significant structural flexibility as shown by the lower hNOE values (Figure S3B).

In the wild-type Pin1 PPIase structure, the W73 indole ring is buried in the cavity formed by $\alpha2-\alpha3$ helices (Figure S2B).[11] As seen in the comparison of the structures (Figure S2B), the C113A mutant causes structural changes to the $\alpha2-\alpha3$ loop (Figure S2A), which releases the W73 indole ring from the interhelix cavity (Figure S2B). This structural change specifically found in the C113A mutant explains the reduced hNOE values for residues W73−Q75 in the C113A mutant (Figure S3B).

Protonation States of Histidines H59 and H157 Change in the C113A and C113S Mutants. The histidines in the dual-histidine motif engage in the hydrogen bond network, in which H59 and H157 are in ε- and δ-tautomers, respectively.[16,17] In our previous work, we showed that impairing the hydrogen bond between H59 and H157 destabilized the structure.[17] The change in the protonation states of the histidines, which is theoretically predicted to occur according to the state of C113,[20] should have a significant impact on the structure and dynamics of these residues. According to the simulation,[20] mutation of C113 should change the protonation states of H59 and H157.

The imidazole rings of H59 and H157 in the C113A mutant gave no correlations in the multibond $^{1}H-^{15}N$ HSQC spectrum, whereas the corresponding histidines in the C113S mutant showed faint but detectable signals (Figure 4A, orange). The spectra observed for the histidines in these mutants are quite different from the spectrum recorded on the wild-type protein. Here, the histidines in the wild type gave rise to clear correlations in the spectrum (Figure 4A, black).[17] The spectral changes observed for the histidines in the mutants indicate that the histidines in the mutants are in states different from those in the wild type.

The imidazole $^{15}N^{\varepsilon2}$ and $^{15}N^{\delta1}$ chemical shifts can be used to distinguish protonation states of the histidine side chain.[21] H59 $^{15}N^{\varepsilon2}$ in the C113S mutant showed a broadened signal at ∼180 ppm, suggesting that the H59 imidazole ring is fully protonated as the imidazolium cation (Figure 4A). The imidazolium state usually gives four signals, as observed for H3 in the N-terminally attached GSHM segment of the construct (Figure

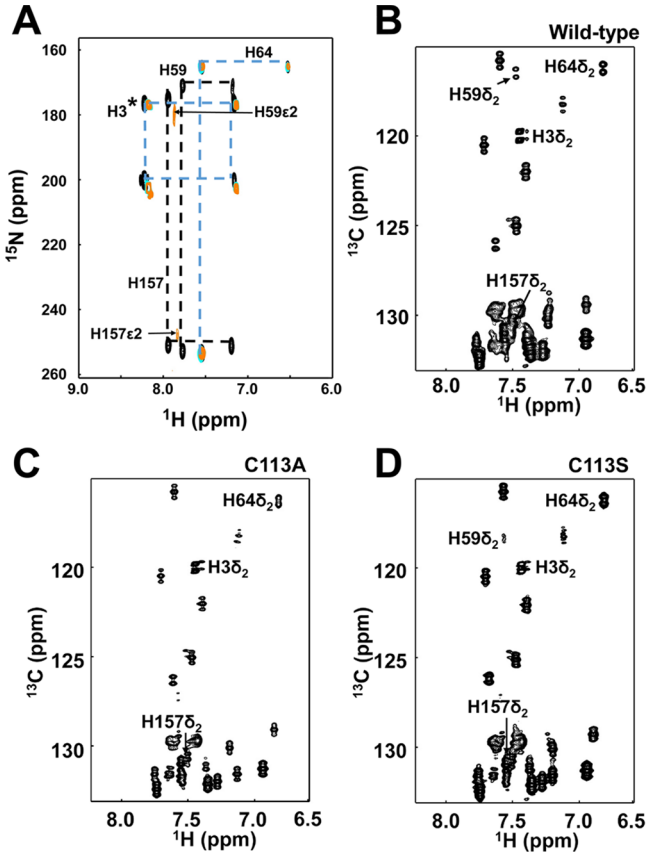

Figure 4. 2D $^{1}H-^{15}N$ multibond HSQC spectra and 2D $^{1}H-^{13}C$ HSQC spectra for the imidazole rings in the Pin1 PPIase domain. (A) 2D $^{1}H-^{15}N$ multibond HSQC spectra for the imidazole rings of the histidines in the wild type (black), C113A (cyan), and C113S (orange). A set of signals marked with an asterisk represent the histidine (termed H3 in the text) located within the N-terminal GSHM segment, which is present because of the expression construct. 2D $^{1}H-^{13}C$ HSQC spectra for (B) the wild type, (C) C113A, and (D) C113S.

4A). The H59 $^{15}N^{\varepsilon2}$ broadened signal suggests the H59 is in chemical exchange between the ε-tautomer (literature value, $\delta^{15}N^{\varepsilon2}$ = 167.5 ppm)[21] and the imidazolium state (literature value, $\delta^{15}N^{\varepsilon2}$ = 176.5 ppm).[27] This is supported by the $^{13}C^{\delta2}$ chemical shift at 118.3 ppm for H59 in the C113S mutant (Figure 4D). Literature values for the imidazole ring in the ε-tautomer give a $^{13}C^{\delta2}$ at 117.9 ppm, whereas the imidazolium state gives a $\delta^{13}C^{\delta2}$ of 120.0 ppm.[21,40] The imidazole $^{13}C^{\delta2}$ value for H59 in the C113S mutant was observed at a ^{13}C chemical shift between the value for the ε-tautomer and imidazolium states (Figure 4D). The $^{13}C^{\delta2}$ signal for H59 was significantly weaker than the corresponding signal in the wild-type protein (Figure 4B), suggesting that the H59 imidazole is in chemical exchange at an intermediate rate on the NMR chemical shift time scale. The state of H59 in the C113S mutant is quite different from that in the wild type (Figure 4D), as clearly seen upon comparison of the spectrum of the wild-type protein, where H59 $^{13}C^{\delta2}$ resonates at ∼116 ppm, a typical position for the ε-tautomer (Figure 4B).

H157 in the C113S mutant showed a broadened $^{15}N^{\varepsilon2}$ signal at ∼250 ppm, indicating that H157 is in the δ-tautomer state (literature value, $\delta N^{\varepsilon2}$ = 249.5 ppm) (Figure 4A).[21] $^{13}C^{\delta2}$ for H157 resonates at 129.6 ppm, which is close to the literature value for the δ-tautomer (127.1 ppm) (Figure 4D).[40] The

DOI: 10.1021/acs.biochem.5b00606
Biochemistry 2015, 54, 5242−5253

broadened $^{1}H-^{15}N$ correlation for the H157 imidazole ring in the C113S mutant, therefore, is presumably caused by the imidazole ring fluctuating at a rate that facilitates ^{15}N transverse relaxation (Figure 4A).

The C113A mutant did not give correlations for H59 and H157 in the multibond $^{1}H-^{15}N$ HSQC spectrum (Figure 4A). In a $^{1}H-^{13}C$ HSQC spectrum for the C113A mutant, the H157 $^{13}C^{\delta 2}$ signal was observed, whereas H59 did not show any correlations (Figure 4C). On the basis of the $^{13}C^{\delta 2}$ chemical shift (130.5 ppm), residue H157 adopts the δ-tautomer state (Figure 4C).[21,40] The loss of any $^{1}H-^{15}N$ correlation for H157 is ascribed to ring fluctuations that accelerate the imidazole ^{15}N transverse relaxation and lead to excessive line broadening of the resonances.

We could not detect a $^{1}H-^{13}C^{\delta 2}$ correlation for H59 in the C113A mutant (Figure 4C), even when the spectrum was plotted at the thermal noise threshold (Figure S4). Nonetheless, a $^{1}H-^{13}C^{\varepsilon 1}$ correlation was observed clearly for H59 at 137.0 ppm (Figure S4; not that the signal is folded in the spectrum). It is known that the $^{13}C^{\varepsilon 1}$ chemical shift does not change according to the tautomeric states. The literature value for $^{13}C^{\varepsilon 1}$ is 139.6 ppm irrespective of the tautomeric state of the imidazole ring.[40] On the other hand, the $^{13}C^{\delta 2}$ chemical shift varies according to the tautomeric state: the literature values are 117.9 ppm for the ε-tautomer and 127.1 ppm for the δ-tautomer.[40]

For H59 in the C113A mutant, a $^{1}H-^{13}C$ correlation for $^{13}C^{\varepsilon 1}$ was observed, while the signal for $^{13}C^{\delta 2}$ was not observed (Figure S4). This unusual observation can be explained by chemical exchange between the ε- and δ-tautomers for H59. If the exchange rate is close to the chemical shift differences between the ε- and δ-tautomers, the $^{1}H-^{13}C^{\delta 2}$ signal significantly broadens and is no longer detectable.[41] The $^{1}H-^{13}C^{\varepsilon 1}$ signal can be observed even when the imidazole ring is undergoing chemical exchange, because the $^{13}C^{\varepsilon 1}$ shift does not change according to the tautomeric state.[40] Therefore, residue H59 in the C113A mutant is considered to be undergoing chemical exchange between ε- and δ-tautomers.

We should add a comment with regard to the determination of the structure of the C113A and C113S mutants. In the structure determination presented here, the H59 side chain was fixed in the ε-tautomer state, as observed in the wild-type protein structure, and chemical exchange between states was not considered. Although this assumption can be seen as being too simplistic, we were able to determine the structures successfully without any serious violations from the experimental restraints and steric clashes. This is because all the distance restraints for the imidazole ring of H59 were from the covalent ring protons in both the C113A and C113S mutants (Figure S5).

C113A and C113S Mutations Cause Different Structural Changes in the Active Site. The C113A and C113S mutations have different active site structures (Figure 5). An expanded view of the active site of the C113S mutant shows that the imidazole rings of H59 and H157 are in orientations different from those in the wild-type protein, whereas the corresponding histidines in the C113A mutant adopt similar orientations (Figure 5A). Comparison of the distributions of χ_2 angles for H59 and H157 among the 10 lowest-energy NMR structures (Figure S5) shows that the observed changes in the imidazole ring orientations in the C113S mutant are statistically significant (Figure 5B and Table S2).

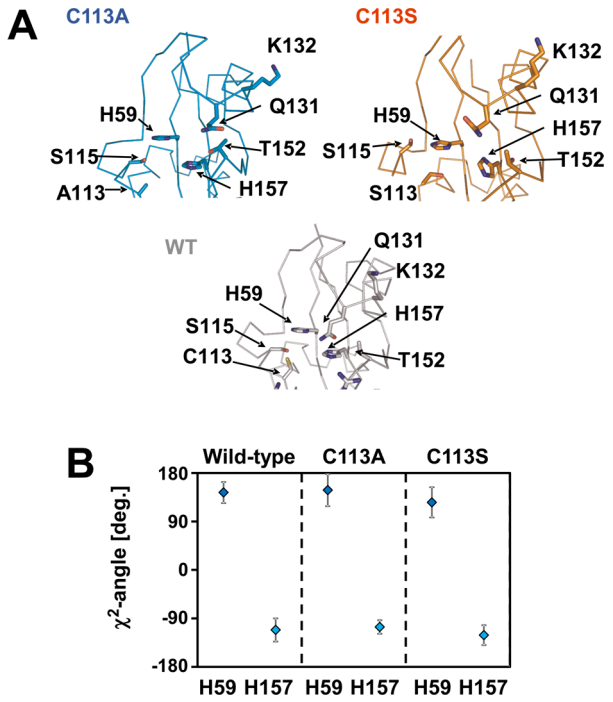

Figure 5. Comparison of the active site structures. (A) Close-up views of the C113A (cyan) and C113S (orange) mutants with the wild type (gray). (B) χ^2 angle distributions for H59 and H157 among the 10 lowest-energy NMR structures for the wild type, C113A, and C113S. The diamond represents the average value and the error bar the magnitude of the corresponding standard deviation.

Structural changes caused by C113A and C113S mutations were examined by comparing the Cα atom positions relative to those of the wild type (Figure 6A). The profiles for the Cα displacement showed that the mutants shared the major structural changes to the $\beta 1-\alpha 1$ loop. The C113A mutant showed additional structural changes near the $\beta 3-\beta 4$ loop (Figure 6A), which is consistent with the enhanced H/D exchange rates and the significantly reduced signal intensities for the corresponding residues characteristically observed for the C113A mutant (Figure 7 and Figure S6). The C113A mutation affects residues farther away in the primary sequence from the mutation site when compared with the C113S mutant. This observation is consistent with the chemical shift differences that showed greater values in the $\beta 3-\beta 4$ loop for the C113A mutant when compared with the results for the C113S mutant (Figure 2).

Inter-residue Cα and Cβ distances for selected residues in the active site were compared (Figure 6B). In the C113A mutant, the S115–H59 distance was shortened, while residues A113 and S154 are farther apart relative to the corresponding distances in the wild-type protein (Figure 6B). The increase in distance between residues A113 and S154 in the C113A mutant resembles the theoretically computed change to the active site structure of the wild type when residue C113 transforms into the thiol form.[20] In the simulation by Barman and Hamelberg, the C113–S154 distance increases in association with a change in the protonation state of H59 from the ε- to δ-tautomer by forming a hydrogen bond between S115 and H59.[20] The shortened S115–H59 distance observed in the C113A mutant suggests a hydrogen bond forms between S115 and H59, as predicted in the simulation.[20]

DOI: 10.1021/acs.biochem.5b00606
Biochemistry 2015, 54, 5242–5253

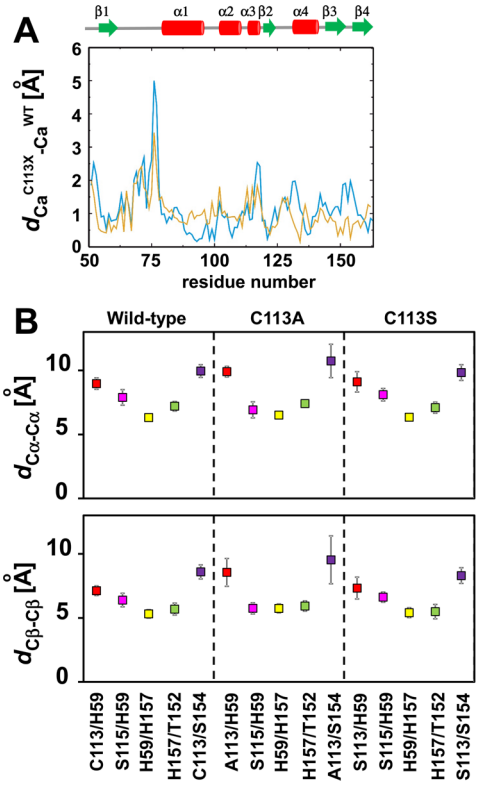

Figure 6. Structural changes measured by the Cα−Cα and Cβ−Cβ distances. (A) Displacement of Cα positions in the C113A (cyan) and C113S (orange) mutants relative to the corresponding Cα atoms in the wild-type protein. (B) Distributions of Cα−Cα and Cβ−Cβ distances among the 10 lowest-energy NMR structures for selected pairs of residues in wild-type Pin1, C113A, and C113S.

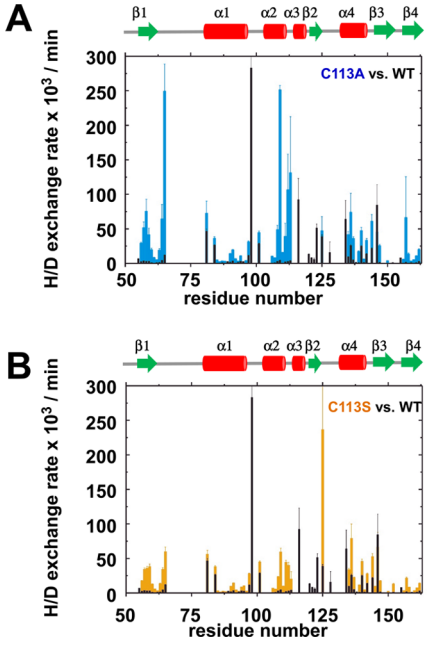

Figure 7. Plot of the H/D exchange rates for residues of the (A) C113A mutant (cyan) and (B) C113S mutant (orange), and the corresponding values determined for the wild-type protein (black).

The C113S mutation does not change the spatial arrangement of the active site residues, including H59, S113, S115, T152, S154, and H157 (Figure 6B). S115 may form a hydrogen bond to S113, instead of H59, as theoretically predicted in the wild type, which adopts the C113 thiol form.[20] The C113S mutant, therefore, maintains the narrow active site entrance as found in the apo state of the wild type, which is a key structural difference from the C113A mutant.

Changes in the Structural Dynamics of the C113A and C113S Mutants. The backbone dynamics of the C113A and C113S mutants were found to differ from that of wild-type Pin1, as measured by the reduced spectral densities.[42,43] The C113A mutation caused an increase in the $J_{eff}(0)$ values for most of the residues in the PPIase domain; $\Delta J_{eff}(0) = J_{eff}(0)^{C113A/S} - J_{eff}(0)^{wild}$ (Figure 8A). Residues with increased $J_{eff}(0)$ values were found to be primarily clustered in the $\beta1-\alpha1$ loop (Figure 8A). The increase in the $J_{eff}(0)$ value implies that the corresponding residues have promoted backbone motions on the microsecond to millisecond time scale relative to the wild type.[42] The loss of a hydrogen bond between C113 and H59 caused by the C113A mutation appears to have destabilized the active site structure to induce slower backbone fluctuations to residues in the active site (Figure 8A). In contrast to C113A, the C113S mutant showed rather randomly distributed $\Delta J_{eff}(0)$ values (Figure 8B); the C113S mutation did not induce backbone motions for active site residues on the microsecond to millisecond time scale.

The profile of $\Delta J(\omega_N) = J(\omega_N)^{C113A/S} - J(\omega_N)^{wild}$ for the C113S mutant differed from the profile for the C113A mutant (Figure 8C,D). The C113S mutant showed positive $\Delta J(\omega_N)$ values for most residues, whereas the $\Delta J(\omega_N)$ values for the C113A mutant were both negative and positive with a less biased distribution (Figure 8C,D).

To characterize the significance of the difference in $\Delta J(\omega_N)$ distributions, we compared the Lipari−Szabo maps for $J(\omega_h)$ and $J(\omega_N)$ among the three proteins (Figure S7A).[44] In the Lipari−Szabo model-free formalism, the spectral density function for the motion of a given N−H bond vector is described by

$$J(\omega) = \frac{2}{5}\left(\frac{S^2\tau_m}{1+\omega^2{\tau_m}^2} + (1-S^2)\frac{\tau}{1+\omega^2\tau^2}\right) \quad (2)$$

$$1/\tau = 1/\tau_m + 1/\tau_e \quad (3)$$

where S^2 is a measure of the spatial restriction of internal motion, τ_e is the correlation time to describe the time scale of internal motion, and τ_m is the rotational correlation time for overall molecular tumbling.[45]

In the three proteins, the most residues showed $[J(\omega_N), J(\omega_h)]$ plots close to the rigid isotropic tumbling curve or the "$\tau_e = 0$" line (Figure S7A): the "$\tau_e = 0$" line is defined as the line passing through the rigid isotropic tumbling point with a τ_m of 9.5 ns, which corresponds to $[J^{rigid}(\omega_N), J^{rigid}(\omega_h)] = (0.20, 0.02)$, to the origin (Figure S7B). The increase in $J(\omega_N)$ is, therefore, mainly explained by the increasing correlation time for the internal motion, τ_e, with a small change in S^2.

The $J(\omega_N)$ values for the residues in the C113S mutant are greater than those for the wild-type and C113A mutant Pin1; statistical significance was assessed by the t test, with a p value of <0.01 (Figure S7C,D). The residues in the C113S mutant tend to have greater τ_e values, indicating that the C113S mutant structure has overall reduced local backbone motions in the nanosecond to picosecond time regime relative to those of the wild-type protein and the C113A mutant (Figure 8D).

DOI: 10.1021/acs.biochem.5b00606
Biochemistry 2015, 54, 5242−5253

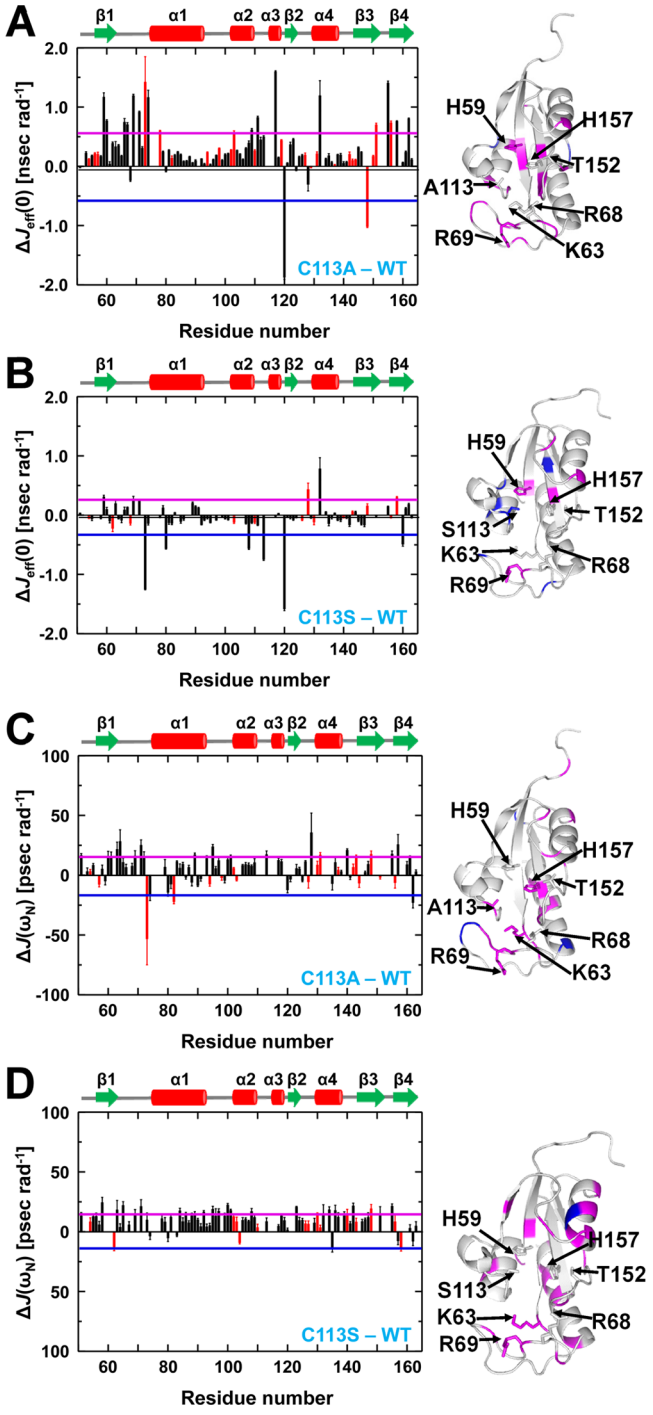

Figure 8. Plots of the differences in spectral density values. $\Delta J_{eff}(0)$ is defined as $J_{eff}(0)^{C113A/S} - J_{eff}(0)^{wild}$, and $\Delta J(\omega_N) = J(\omega_N)^{C113A/S} - J(\omega_N)^{wild}$. $\Delta J_{eff}(0)$ plots for (A) C113A and (B) C113S. $\Delta J(\omega_N)$ values plotted for (C) C113A and (D) C113S. The red and black bars represent residues that show extreme narrowing limit backbone motion [$J(\omega_N) < 0.2$] (red) and residues for which $J(\omega_N) \geq J^{rigid}(\omega_N) = 0.2$ (black). Residues are color-coded according to the magnitudes of the differences in spectral densities ΔJ: residues for which $\Delta J > \Delta J^{ave} + 0.5\sigma$ are colored magenta, while those for which $\Delta J < \Delta J^{ave} - 0.5\sigma$ are colored blue, where ΔJ^{ave} and σ are the average of the ΔJ values and the standard deviation, respectively.

DISCUSSION

Barman and Hamelberg have theoretically computed that the hydrogen bond network in the active site of Pin1 PPIase is dynamically modulated according to the protonation state of C113.[20] Here, C113 remains as a thiolate form in the apo state but becomes protonated or changes to the thiol form upon binding to the *cis* substrate.[20] This study also shows that changes in the active site structure and the dynamics associated with the rearrangement of the hydrogen bond network facilitate the isomerization process.[20] Their theoretical insights into the Pin1 PPIase isomerization mechanism provided the impetus of this study to examine how amino acid mutations to C113 modulate the hydrogen bond network.

The Dynamics of the Hydrogen Bond Network Changed According to the Type of Amino Acid at Position 113. The changes in the dynamics of the hydrogen bond network caused by C113A and C113S mutations are schematically summarized in Figure 9. In our previous work, we clearly identified the tautomeric states of H59 and H157 in the wild type by multibond $^{1}H-^{15}N$ HSQC analysis, which showed that H59 and H157 are ε- and δ-tautomers, respectively (Figure 9A).[17] The results are consistent with the tautomers of the corresponding histidines identified in the high-resolution crystal structure of Par14, a PPIase homologous to Pin1.[16] Our NMR results showed that the hydrogen bond network exists as in the Par14 crystal structure; however, NMR could not directly observe the sample if C113 was in the thiolate or thiol form.[17]

As described in the Results, the unusual $^{1}H-^{15}N$ and $^{1}H-^{13}C$ HSQC spectra for the imidazole rings in the mutants could represent chemical exchange between the different protonation states of the H59 imidazole ring (Figure 9B,C).

The C113A mutant lacks a hydrogen bond between H59 and A113 and may be stabilized by H59 adopting the δ-tautomer state by hydrogen bonding with S115 (Figure 9B). The hydrogen bond from S115 to H59 was theoretically predicted in association with the conversion from thiolate to thiol in C113 and its release from interaction with H59.[20] In a 2D $^{1}H-^{15}N$ HSQC spectrum for the C113A mutant, the correlation representing S115 was not observed, while the neighboring S114 signal was observed, which indicates that S115 undergoes chemical exchange through interaction with H59 exchanging between ε- and δ-tautomers (Figure 9B).

In the simulation by Barman and Hamelberg, once H59 becomes the δ-tautomer, it prompts the conversion of H157 from the δ- to ε-tautomer with a rearrangement of the hydrogen bond between H157 and the T152 hydroxyl oxygen as the acceptor.[20] The NMR results, however, showed that H157 remains as the δ-tautomer in the C113A mutant (Figure 4). Therefore, there should be a steric clash between H59 (δ-tautomer) and H157 (δ-tautomer) (Figure 9B). As seen in the solution structure of the C113A mutant, the distance between A113 and S154 increased with a concomitant decrease in the S115–H59 distance (Figure 6B). This indicates that S115 attracts H59 by hydrogen bonding to release the steric clash with H157. Because the side chain contacts were alleviated by the widened cavity entrance formed by A113 and S154, the imidazole rings of H59 and H157 maintain an orientation similar to that observed in the wild-type protein (Figure 5). The widened active site structure resembles the theoretically predicted structure present in the wild type with the thiol form of C113.[20] The induced structural deformation in the C113A mutant was also apparent in the CD spectral change (Figure S8A).

The C113S mutant showed chemical exchange for H59 between the ε-tautomer and the imidazolium state (Figure 9C). On the basis of the $^{15}N^{\varepsilon 1}$ and $^{13}C^{\delta 2}$ chemical shifts, it is most

DOI: 10.1021/acs.biochem.5b00606
Biochemistry 2015, 54, 5242–5253

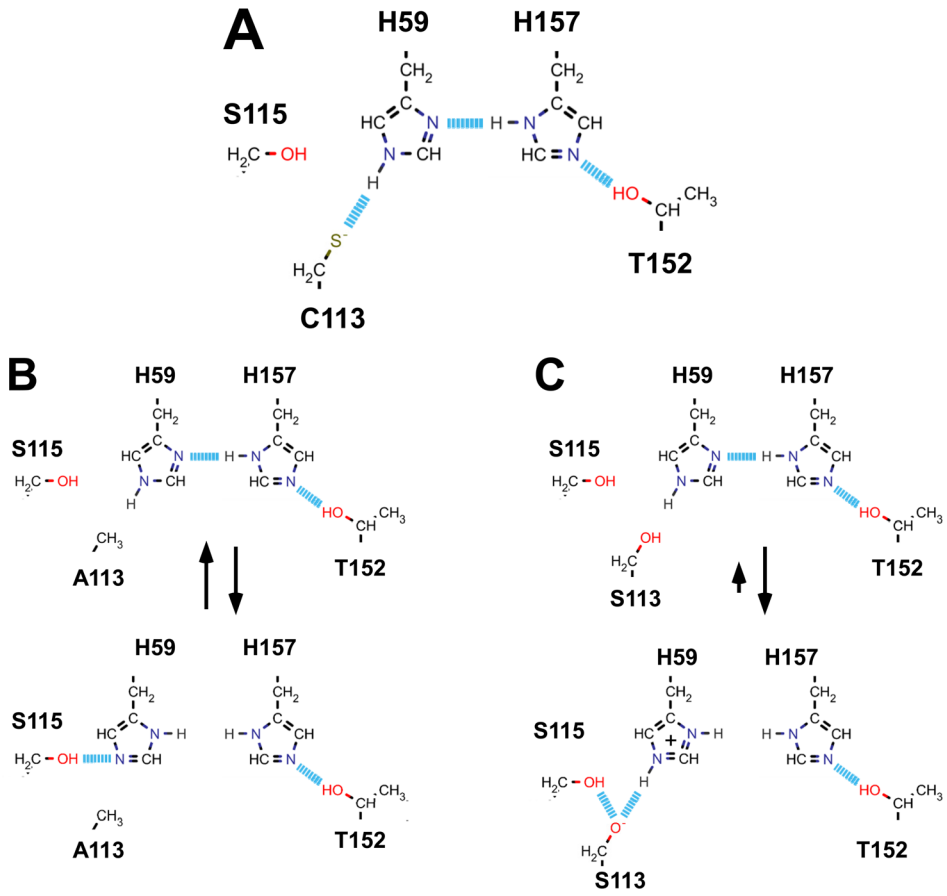

Figure 9. Dynamics of the hydrogen bond network. (A) Hydrogen bond network identified in the wild-type Pin1 PPIase according to the high-resolution crystal structure of Par14[16], where C113 is drawn to position the thiolate as theoretically proposed.[20] (B) Hydrogen bond rearrangement associated with the exchange of H59 between the ε- and δ-tautomers. (C) Rearrangement of the hydrogen bond network caused by the conversion of the H59 ε-tautomer to the imidazolium form.

probable that H59 preferentially stays in the imidazolium state (Figure 4). The imidazolium could be stabilized by hydrogen bonding with the S113 hydroxyl group (Figure 9C). In addition, S113 hydrogen bonding to H59 could be stabilized by the interaction with S115, as predicted in the simulation in which S115 hydrogen bonds to the thiol sulfur in C113 (Figure 9C). The predicted hydrogen bonding of S115 to S113 might be supported by the change in the signal intensity of S115 on a $^{1}H-^{15}N$ HSQC spectra (Figure S6): the $^{1}H-^{15}N$ HSQC signal for S115 was not observed for the C113A mutant, while it was detected for the C113S mutant, which most probably means that the backbone fluctuation of the S115 residue was alleviated through the hydrogen bonding to the neighboring residue.

It is noted that in the simulation on the wild-type Pin1 bound to the substrate, the thiol moiety of C113 is engaged in an interaction with the substrate rather than an intramolecular hydrogen bond to H59; thus, the wild type should not generate the imidazolium at H59.[20]

H157 remains in the δ-tautomer, which is evident in the NMR spectra (Figure 4). The C113S mutant did not show any significant change to the active site backbone structure, as seen from the Cα distances among the selected residues (Figure 6B). Because there is a minimal change in the backbone structure of the active site of the C113S mutant, steric clashes between the imidazole rings of H59 (imidazolium) and H157 (δ-tautomer) were mitigated by the change in their side chain orientations (Figure 5).

In the schemes for both mutants, the hydrogen bond between H59 and H157 will be broken transiently in exchanging between the different imidazole states of H59 (Figure 9B,C). The breakage of the hydrogen bond in the dual-histidine motif explains the further reduced structural stabilities of C113A and C113S relative to the C113D mutant (Table 1 and Figure S8).

It is interesting to note that the overlay of the CD spectra for the wild type and C113D, C113A, and C113S mutants showed an isosbestic point around 208 nm (Figure S8A). Taking into consideration the significantly deformed active site structure to give an open entrance architecture in the C113A mutant (Figure 6B), we postulate that the Pin1 PPIase domain can adopt two major conformations with different entrance forms in the active site: an open state (as in the C113A mutant) and a closed state (as in the wild type). This explains the differences in the CD spectra showing an isosbestic point among the four types of Pin1 PPIase proteins (Figure S8A).

C113A and C113S Mutations Induced Different Structural Dynamics. We also found that mutation of C113 caused different structural dynamics on various time scale regimes.

The C113A mutation induced additional backbone motion on the millisecond to microsecond time scale, as evident by the increase in the $J_{eff}(0)$ values for most residues (Figure 8A). The change was similar to that observed for the C113D mutant, but the C113A mutation caused a significant increase in $J_{eff}(0)$

DOI: 10.1021/acs.biochem.5b00606
Biochemistry 2015, 54, 5242−5253

values for residues in the β4 strand, which was not apparent in the C113D mutant.[17] Impairing the structural stability of the β4 strand is a characteristic feature of the C113A mutant, which is evident in the enhanced H/D exchange rates for residues in this strand (Figure 7A). As shown in the solution structure comparison, the rearrangement of the hydrogen bond network in the C113A mutant is associated with a change in structure of the active site entrance (Figure 6B), which may cause structural perturbations to the β4 strand: the active site entrance includes S154 in the β3−β4 loop. The enhanced structural dynamics on the millisecond to microsecond time scale may be understood by considering that the C113A mutant creates a vacant cavity in the active site, which is occupied by the longer side chain of cysteine in the wild-type protein (Figure 9B).

The C113S mutant caused different changes in structural dynamics with changes apparent in the nanosecond to picosecond time regime, as seen by the increase in $J(\omega_N)$ values (Figure 8D). The changes in $J(\omega_N)$ values for the C113S mutant imply that residues with increased $J(\omega_N)$ values had a reduced level of local motion, thus adopting more rigid local structures relative to the corresponding residues in the wild-type protein (Figure 8D). This change may arise from the tightly packed imidazole rings of H59 and H157 in the active site cavity; both residues have the $N^{\delta 1}H$ moiety sterically crowded in the cavity (Figure 9C).

The observed change in the dynamics for each mutant can be explained by assuming the protonation dynamics of H59 and the associated changes in the interaction with H157 (Figure 9). Our proposed imidazole dynamics of H59 in the mutants are consistent with the NMR data collected in this study and supported by the theoretically predicted dynamic hydrogen bond network described by Barman and Hamelberg.[20]

Why Does the C113S Mutant Have an Isomerization Rate Lower Than That of the C113A Mutant? The C113A and C113S mutants are reported to have reduced isomerase activities.[11,13] Direct determination of the isomerization rates by EXSY experiments demonstrated that the C113S mutant has a significantly reduced isomerization rate when compared with the rate measured for the C113A mutant (Table 1).

The C113A and C113S mutants have an altered basic triad structure in the active loop (Figure 5A), which explains their reduced substrate affinity. The change in the basic triad structure was also found for the C113D mutant.[17] The C113D mutant, however, kept the hydrogen bonding network as in the wild type.[17] Because the isomerization rate of the C113A mutant is close to the rate observed for the C113D mutant, the reduced isomerization activity of C113A can be solely ascribed to the weakened substrate binding ability caused by the structural change in the basic triad. In other words, the change in the hydrogen bonding network surrounding H59 should have a marginal impact on the isomerization process (Figure 9B).

The C113S mutant showed similar structural change in the basic triad and therefore a reduced substrate affinity, as in the case of the C113A mutant (Figure 3B). In contrast to the C113A mutant, the change in the protonation states of H59 in the C113S mutant (Figure 9C) could further reduce the isomerization rate (Table 1). The altered orientation of the H59 and H157 imidazole rings (Figure 5A) and the presence of the H59 imidazolium form (Figure 9C) should be prohibitive to the isomerization reaction. H59 and H157 constitute the floor in the active site that holds the Pro residue of the substrate in position for catalysis. The disorientation of the histidine rings may impair the interaction with the Pro residue.[14] As seen in the crystal structure,[14] the Pro residue of the substrate is stabilized by binding into a hydrophobic catalytic cavity. A charged imidazolium H59 occurring during chemical exchange, therefore, will also likely diminish substrate affinity (Figure 9C). The changes in the catalytic cavity could explain the further reduction in the isomerization rate of the C113S mutant.

It is intriguing to note that the change in the protonation states of H59 in the C113A mutant (Figure 9B) appears to have little effect on the isomerization process in contrast to the case for the C113S mutant (Figure 9C). In the C113A mutant, H59 is supposed to make the hydrogen bond to S115 with conversion from ε- to δ-tautomeric states (Figure 9B). This suggests that the observed conversion for the H59 protonation states in the C113A mutant (Figure 9B) is compatible with the isomerization, being consistent with the reaction process proposed by the simulation.[20]

In summary, the *cis*−*trans* isomerization in Pin1 PPIase is mediated through the binding to the phosphor moiety by the basic triad in the active loop and followed by the conversion in the protonation states of the dual histidines H59 and H157. These results emphasize the conversion in the protonation states of the dual histidine is essential for the isomerization and the process depends on the residue type at position 113. This work supports the theoretically predicted mechanism that C113-mediated rearrangement of the hydrogen bonding network in the active site prompts the isomerization reaction.[20]

CONCLUSIONS

In this work, using the C113A and C113S mutants of the Pin1 PPIase domain, we found the dynamics in the hydrogen bond network mediated by H59 and H157 (dual-histidine motif) can change according to the residue type at position 113. The absence of resonances or severely reduced signal intensities for resonances representing H59 and H157 in the mutants provided evidence of dynamic rearrangement of the hydrogen bond network, as theoretically predicted.[20] The plausible hydrogen bond dynamics were derived from $^{1}H-^{15}N$ and $^{1}H-^{13}C$ correlations (Figure 9), although incomplete sets of their signals limited our analysis and discussion (Figure 4).

Despite the challenge of observing signals representing the two His residues that constitute the dual-histidine motif, the solution structures, the structural dynamics, and H/D exchange rates for the mutants were found to be consistent with our proposed dynamics in hydrogen bonding among residues A113/S113, S115, H157, and H59 (Figure 9), which supports our models that describe the dynamic hydrogen bond network of the mutants.

Overall, this work experimentally supports the view that the chemical state of C113 plays a pivotal role in reorganizing the hydrogen bond network to facilitate the isomerization process, which was originally proposed by theoretical simulations.[16]

ASSOCIATED CONTENT

Supporting Information

The Supporting Information is available free of charge on the ACS Publications website at DOI: 10.1021/acs.biochem.5b00606.

Tables S1 and S2, Figures S1−S8 (as mentioned in the text), and profiles for the difference spectral density $\Delta J(\omega_h)$ for the C113A and C113S mutants (PDF)

DOI: 10.1021/acs.biochem.5b00606
Biochemistry 2015, 54, 5242−5253

AUTHOR INFORMATION

Corresponding Author

*Department of Mathematical and Life Sciences, School of Science, Hiroshima University, 1-3-1 Kagamiyama, Higashi-Hiroshima 739-8526, Japan. Telephone: +81-82-424-7387. E-mail: tate@hiroshima-u.ac.jp.

Funding

This work is supported by the Platform for Dynamic Approaches to Living System from the Ministry of Education, Culture, Sports, Science and Technology (MEXT), Japan. S.-i.T. also acknowledges support from a Grant-in-Aid for Scientific Research (B) (Grant 26291015) and a Grant-in-Aid for Exploratory Research (Grant 26650023) from the Japan Society for the Promotion of Science (JSPS). J.W. acknowledges support from the China Scholarship Council (CSC, 20120811702).

Notes

The authors declare no competing financial interest.

ACKNOWLEDGMENTS

We acknowledge the Natural Science Center for Basic Research and Development (N-BARD) at Hiroshima University for the use of instruments. We thank Mr. Jun-ichi Kakimura (N-BARD) for his help during NMR data collection.

ABBREVIATIONS

Pin1, peptidyl-prolyl *cis-trans* isomerase NIMA-interacting 1; PPIase, peptidyl-prolyl isomerase; HSQC, heteronuclear single-quantum correlation; CD, circular dichroism; NMR, nuclear magnetic resonance; EXSY, exchange spectroscopy; CPMG, Carr−Purcell−Meiboom−Gill; EDTA, ethylenediaminetetraacetic acid; DTT, dithiothreitol; BMRB, Biological Magnetic Resonance Bank; PDB, Protein Data Bank; rmsd, root-mean-square deviation.

REFERENCES

(1) Yaffe, M. B., Schutkowski, M., Shen, M., Zhou, X. Z., Stukenberg, P. T., Rahfeld, J.-U., Xu, J., Kuang, J., Kirschner, M. W., Fischer, G., Cantley, L. C., and Lu, K. P. (1997) Sequence-Specific and Phosphorylation-Dependent Proline Isomerization: A Potential Mitotic Regulatory Mechanism. *Science 278*, 1957−1960.

(2) Lu, Z., and Hunter, T. (2014) Prolyl isomerase Pin1 in cancer. *Cell Res. 24*, 1033−1049.

(3) Lu, K. P. (2004) Pinning down cell signaling, cancer and Alzheimer's disease. *Trends Biochem. Sci. 29*, 200−209.

(4) Lu, K. P., and Zhou, X. Z. (2007) The prolyl isomerase PIN1: a pivotal new twist in phosphorylation signalling and disease. *Nat. Rev. Mol. Cell Biol. 8*, 904−916.

(5) Lu, K. P., Liou, Y. C., and Zhou, X. Z. (2002) Pinning down proline-directed phosphorylation signaling. *Trends Cell Biol. 12*, 164−172.

(6) Blume-Jensen, P., and Hunter, T. (2001) Oncogenic kinase signalling. *Nature 411*, 355−365.

(7) Sultana, R., Boyd-Kimball, D., Poon, H. F., Cai, J., Pierce, W. M., Klein, J. B., Markesbery, W. R., Zhou, X. Z., Lu, K. P., and Butterfield, D. A. (2006) Oxidative modification and down-regulation of Pin1 in Alzheimer's disease hippocampus: A redox proteomics analysis. *Neurobiol. Aging 27*, 918−925.

(8) Lim, J., and Ping Lu, K. (2005) Pinning down phosphorylated tau and tauopathies. *Biochim. Biophys. Acta, Mol. Basis Dis. 1739*, 311−322.

(9) Balastik, M., Lim, J., Pastorino, L., and Lu, K. P. (2007) Pin1 in Alzheimer's disease: Multiple substrates, one regulatory mechanism? *Biochim. Biophys. Acta, Mol. Basis Dis. 1772*, 422−429.

(10) Theuerkorn, M., Fischer, G., and Schiene-Fischer, C. (2011) Prolyl cis/trans isomerase signalling pathways in cancer. *Curr. Opin. Pharmacol. 11*, 281−287.

(11) Ranganathan, R., Lu, K. P., Hunter, T., and Noel, J. P. (1997) Structural and Functional Analysis of the Mitotic Rotamase Pin1 Suggests Substrate Recognition Is Phosphorylation Dependent. *Cell 89*, 875−886.

(12) Xu, G. G., Zhang, Y., Mercedes-Camacho, A. Y., and Etzkorn, F. A. (2011) A reduced-amide inhibitor of Pin1 binds in a conformation resembling a twisted-amide transition state. *Biochemistry 50*, 9545−9550.

(13) Behrsin, C. D., Bailey, M. L., Bateman, K. S., Hamilton, K. S., Wahl, L. M., Brandl, C. J., Shilton, B. H., and Litchfield, D. W. (2007) Functionally important residues in the peptidyl-prolyl isomerase Pin1 revealed by unigenic evolution. *J. Mol. Biol. 365*, 1143−1162.

(14) Mercedes-Camacho, A. Y., Mullins, A. B., Mason, M. D., Xu, G. G., Mahoney, B. J., Wang, X., Peng, J. W., and Etzkorn, F. A. (2013) Kinetic Isotope Effects Support the Twisted Amide Mechanism of Pin1 Peptidyl-Prolyl Isomerase. *Biochemistry 52*, 7707−7713.

(15) Fischer, S., Michnick, S., and Karplus, M. (1993) A mechanism for rotamase catalysis by the FK506 binding protein (FKBP). *Biochemistry 32*, 13830−13837.

(16) Mueller, J. W., Link, N. M., Matena, A., Hoppstock, L., Ruppel, A., Bayer, P., and Blankenfeldt, W. (2011) Crystallographic proof for an extended hydrogen-bonding network in small prolyl isomerases. *J. Am. Chem. Soc. 133*, 20096−20099.

(17) Xu, N., Tochio, N., Wang, J., Tamari, Y., Uewaki, J.-i., Utsunomiya-Tate, N., Igarashi, K., Shiraki, T., Kobayashi, N., and Tate, S.-i. (2014) The C113D Mutation in Human Pin1 Causes Allosteric Structural Changes in the Phosphate Binding Pocket of the PPIase Domain through the Tug of War in the Dual-Histidine Motif. *Biochemistry 53*, 5568−5578.

(18) Hennig, L., Christner, C., Kipping, M., Schelbert, B., Rücknagel, K. P., Grabley, S., Küllertz, G., and Fischer, G. (1998) Selective Inactivation of Parvulin-Like Peptidyl-Prolyl cis/trans Isomerases by Juglone. *Biochemistry 37*, 5953−5960.

(19) Sultana, R., Boyd-Kimball, D., Poon, H. F., Cai, J., Pierce, W. M., Klein, J. B., Markesbery, W. R., Zhou, X. Z., Lu, K. P., and Butterfield, D. A. (2006) Oxidative modification and down-regulation of Pin1 in Alzheimer's disease hippocampus: A redox proteomics analysis. *Neurobiol. Aging 27*, 918−925.

(20) Barman, A., and Hamelberg, D. (2014) Cysteine-Mediated Dynamic Hydrogen-Bonding Network in the Active Site of Pin1. *Biochemistry 53*, 3839−3850.

(21) Pelton, J. G., Torchia, D. A., Meadow, N. D., and Roseman, S. (1993) Tautomeric states of the active-site histidines of phosphorylated and unphosphorylated IIIGlc, a signal-transducing protein from escherichia coli, using two-dimensional heteronuclear NMR techniques. *Protein Sci. 2*, 543−558.

(22) Sudmeier, J., Bradshaw, M., Coffman Haddad, K. E., Day, R., Thalhauser, C., Bullock, P., and Bachovchin, W. (2003) Identification of histidine tautomers in proteins by 2D 1H/13Cdelta2 one-bond correlated NMR. *J. Am. Chem. Soc. 125*, 8430−8431.

(23) Zhou, X. Z., Kops, O., Werner, A., Lu, P. J., Shen, M., Stoller, G., Kullertz, G., Stark, M., Fischer, G., and Lu, K. P. (2000) Pin1-dependent prolyl isomerization regulates dephosphorylation of Cdc25C and tau proteins. *Mol. Cell 6*, 873−883.

(24) Cavanagh, J., Fairbrother, W. J., Palmer, A. G., III, and Skelton, N. J. (1996) *Protein NMR Spectroscopy*, Academic Press, Inc., New York.

(25) Delaglio, F., Grzesiek, S., Vuister, G. W., Zhu, G., Pfeifer, J., and Bax, A. (1995) NMRPipe: a multidimensional spectral processing system based on UNIX pipes. *J. Biomol. NMR 6*, 277−293.

(26) Kobayashi, N., Iwahara, J., Koshiba, S., Tomizawa, T., Tochio, N., Güntert, P., Kigawa, T., and Yokoyama, S. (2007) KUJIRA, a package of integrated modules for systematic and interactive analysis of NMR data directed to high-throughput NMR structure studies. *J. Biomol. NMR 39*, 31−52.

DOI: 10.1021/acs.biochem.5b00606
Biochemistry 2015, 54, 5242−5253

(27) Johnson, B. (2004) Using NMRView to Visualize and Analyze the NMR Spectra of Macromolecules. In *Protein NMR Techniques* (Downing, A. K., Ed.) pp 313−352, Humana Press, Totowa, NJ.
(28) Güntert, P. (2004) Automated NMR Structure Calculation with CYANA. In *Protein NMR Techniques* (Downing, A. K., Ed.) pp 353−378, Humana Press, Totowa, NJ.
(29) Güntert, P. (2009) Automated structure determination from NMR spectra. *Eur. Biophys. J. 38*, 129−143.
(30) Shen, Y., Delaglio, F., Cornilescu, G., and Bax, A. (2009) TALOS+: a hybrid method for predicting protein backbone torsion angles from NMR chemical shifts. *J. Biomol. NMR 44*, 213−223.
(31) Schwieters, C. D., Kuszewski, J. J., Tjandra, N., and Marius Clore, G. (2003) The Xplor-NIH NMR molecular structure determination package. *J. Magn. Reson. 160*, 65−73.
(32) Laskowski, R., Rullmann, J., MacArthur, M., Kaptein, R., and Thornton, J. (1996) AQUA and PROCHECK-NMR: Programs for checking the quality of protein structures solved by NMR. *J. Biomol. NMR 8*, 477−486.
(33) Koradi, R., Billeter, M., and Wüthrich, K. (1996) MOLMOL: A program for display and analysis of macromolecular structures. *J. Mol. Graphics 14*, 51−55.
(34) Wilson, K. A., Bouchard, J. J., and Peng, J. W. (2013) Interdomain interactions support interdomain communication in human Pin1. *Biochemistry 52*, 6968−6981.
(35) Jeener, J., Meier, B. H., Bachmann, P., and Ernst, R. R. (1979) Investigation of exchange processes by two - dimensional NMR spectroscopy. *J. Chem. Phys. 71*, 4546−4553.
(36) Farrow, N. A., Muhandiram, R., Singer, A. U., Pascal, S. M., Kay, C. M., Gish, G., Shoelson, S. E., Pawson, T., Forman-Kay, J. D., and Kay, L. E. (1994) Backbone dynamics of a free and phosphopeptide-complexed Src homology 2 domain studied by 15N NMR relaxation. *Biochemistry 33*, 5984−6003.
(37) Long, D., Liu, M., and Yang, D. (2008) Accurately Probing Slow Motions on Millisecond Timescales with a Robust NMR Relaxation Experiment. *J. Am. Chem. Soc. 130*, 2432−2433.
(38) d'Auvergne, E., and Gooley, P. (2008) Optimisation of NMR dynamic models I. Minimisation algorithms and their performance within the model-free and Brownian rotational diffusion spaces. *J. Biomol. NMR 40*, 107−119.
(39) d'Auvergne, E., and Gooley, P. (2008) Optimisation of NMR dynamic models II. A new methodology for the dual optimization of the model-free parameters and the Brownian rotational diffusion tensor. *J. Biomol. NMR 40*, 121−133.
(40) Platzer, G., Okon, M., and McIntosh, L. P. (2014) pH-dependent random coil (1)H, (13)C, and (15)N chemical shifts of the ionizable amino acids: a guide for protein pK a measurements. *J. Biomol. NMR 60*, 109−129.
(41) van de Ven, F. J. M. (1995) *Multidimensional NMR in Liquids*, Wiley-VCH, New York.
(42) Markus, M. A., Dayie, K. T., Matsudaira, P., and Wagner, G. (1996) Local mobility within villin 14T probed via heteronuclear relaxation measurements and a reduced spectral density mapping. *Biochemistry 35*, 1722−1732.
(43) Farrow, N., Zhang, O., Szabo, A., Torchia, D., and Kay, L. (1995) Spectral density function mapping using 15N relaxation data exclusively. *J. Biomol. NMR 6*, 153−162.
(44) Andrec, M., Montelione, G., and Levy, R. (2000) Lipari−Szabo mapping: A graphical approach to Lipari−Szabo analysis of NMR relaxation data using reduced spectral density mapping. *J. Biomol. NMR 18*, 83−100.
(45) Lipari, G., and Szabo, A. (1982) Model-free approach to the interpretation of nuclear magnetic resonance relaxation in macromolecules. 1. Theory and range of validity. *J. Am. Chem. Soc. 104*, 4546−4559.
(46) Garrett, D. S., Seok, Y.-J., Peterkofsky, A., Clore, G. M., and Gronenborn, A. M. (1997) Identification by NMR of the Binding Surface for the Histidine-Containing Phosphocarrier Protein HPr on the N-Terminal Domain of Enzyme I of the Escherichia coli Phosphotransferase System. *Biochemistry 36*, 4393−4398.

DOI: 10.1021/acs.biochem.5b00606
Biochemistry 2015, 54, 5242−5253